**Original citation:**
Perry, David, Parker, Alexander, Page, Ashley and Unwin, Patrick R.. (2016) Electrochemical control of calcium carbonate crystallization and dissolution in nanopipettes. ChemElectroChem, 3 (12). pp. 2212-2220.

**Permanent WRAP URL:**
http://wrap.warwick.ac.uk/85404

**Copyright and reuse:**
The Warwick Research Archive Portal (WRAP) makes this work by researchers of the University of Warwick available open access under the following conditions.  Copyright © and all moral rights to the version of the paper presented here belong to the individual author(s) and/or other copyright owners.  To the extent reasonable and practicable the material made available in WRAP has been checked for eligibility before being made available.

Copies of full items can be used for personal research or study, educational, or not-for profit purposes without prior permission or charge.  Provided that the authors, title and full bibliographic details are credited, a hyperlink and/or URL is given for the original metadata page and the content is not changed in any way.

**Publisher's statement:**
This is the peer reviewed version of the following article: D. Perry, A. S. Parker, A. Page, P. R. Unwin, ChemElectroChem 2016, 3, 2212., which has been published in final form at http://dx.doi.org/10.1002/celc.201600547 . This article may be used for non-commercial purposes in accordance with Wiley Terms and Conditions for Self-Archiving.

**A note on versions:**
The version presented here may differ from the published version or, version of record, if you wish to cite this item you are advised to consult the publisher's version.  Please see the 'permanent WRAP url' above for details on accessing the published version and note that access may require a subscription.

For more information, please contact the WRAP Team at: wrap@warwick.ac.uk

**warwick.ac.uk/lib-publications**

# ARTICLE

# Electrochemical Control of Calcium Carbonate Crystallization and Dissolution in Nanopipettes

David Perry,[a,b,†] Alexander S. Parker,[a,†] Ashley Page,[a,b] and Patrick R. Unwin[a],*

**Abstract:** Electrochemically-controlled nanopipettes are becoming increasingly versatile tools for a diverse range of sequencing, sizing and imaging applications. Herein, the use of nanopipettes to induce and monitor quantitatively crystallization and dissolution in real time is considered, using $CaCO_3$ in aqueous solution as an exemplar system. The bias between a quasi-reference counter electrode (QRCE) in a nanopipette and one in a bulk solution, is used to mix (or de-mix) two different solutions by ion migration and drive either growth or dissolution depending on the polarity. Furthermore, Raman spectroscopy can be applied simultaneously to identify polymorphs formed in the nanopipette. The technique is supported with a robust finite element method (FEM) model that allows the extraction of time-dependent saturation levels and mixing characteristics at the nanoscale. The technique shows great promise as a tool for rapidly screening growth additives and inhibitors, allowing eight different additives to be ranked in order of efficacy for crystal growth rate inhibition.

## Introduction

Nanopipettes, under electrochemical control, are increasingly becoming powerful tools for a host of analytical applications because of their ease of manufacture and low cost, as well as their versatility, being adaptable to suit a wide range of different configurations. To date, applications of nanopipettes have included use as sensors for a variety of different analytes,[1] as well as tools for local delivery of molecules, achieved by varying the electric field at the end of the nanopipette to trap or release charged species.[2] Additionally they serve as powerful probes for electrochemical reaction, surface charge and topographical imaging[3] as well as other diverse applications, such as enabling the nanobiopsy of living cells[4] and electrospray analysis.[5]

Herein, nanopipettes are used as a reaction centre to study crystallization events on the nanoscale, with the aim of measuring the initial rates of calcium carbonate, $CaCO_3$, growth and dissolution. With the versatile approach presented, multiple growth and dissolution events can be induced and monitored repetitively and reversibly (at will) on a rapid timescale. We

selected $CaCO_3$ for study given its significance in many areas, from being one of the most abundant minerals on Earth,[6] to its use as a biomineral by organisms in the formation of eggshells, seashells, snail shells and skeletal matter.[7] $CaCO_3$ is a significant component of coral reefs[8] and serves as a repository for carbon dioxide.[9] There is also great interest in understanding and preventing the formation of $CaCO_3$ limescale, especially through the use of additives.[10]

$CaCO_3$ crystallization is achieved by filling a nanopipette with a bicarbonate solution (for example) and a quasi-reference counter electrode (QRCE) and applying a bias between this electrode and another QRCE, in a bulk solution of calcium chloride into which the nanopipette is placed. Changing the magnitude and polarity of the bias applied, gives control over the local mixing of $Ca^{2+}$ and $CO_3^{2-}$ ions at the end of the nanopipette, such that growth or dissolution of $CaCO_3$ can be driven. Simultaneously, the ionic current through the end of the nanopipette is sensitive to these events and can be monitored with high time resolution. This approach builds on earlier work that considered the crystallization of zinc phosphate in a nanopipette, showing that the current through the nanopipette was sensitive to growth events and that this process could be manipulated through alteration of the local electric field.[11] Our work develops and advances this methodology significantly and puts it on a quantitative footing. In particular, the use of FEM modeling, allows for an understanding of the mixing processes occurring at the end of the nanopipette and the analysis of the experimental growth (and dissolution) rates, which we are able to follow on a faster timescale. The growth process is typically complete within a few hundred ms. Moreover, the possibility of utilizing Raman spectroscopy in-situ is briefly explored and it is shown that this can allow for further polymorphic identification of the $CaCO_3$ material that forms in the end of the nanopipette.

Finally, a key strength, and new feature, of the approach described in this paper is that the effects of additives can readily be studied, on a fast timescale, from which a ranking of efficacy can be obtained. This capability could have a great impact as it provides a platform wherein nanopipettes could cheaply and robustly be used as a screening tool to discover, and assess, new additives very quickly.

## Results and Discussion

### Growth of Calcium Carbonate in a Nanopipette under Electrochemical Control

The principles of using a single barreled nanopipette for the study of calcium carbonate nucleation and growth are depicted in Figure 1a and b. For most studies, the nanopipette was filled with 125 mM $NaHCO_3$ and placed in a bath of 25 mM $CaCl_2$ (both solutions fixed at pH 9.2) while applying a bias of 4 V to a QRCE in the nanopipette with respect to the QRCE in bulk solution. In this state, a steady current was observed corresponding to an unblocked nanopipette. The tip potential was then switched to -0.25 V to drive $CO_3^{2-}$ (and $HCO_3^-$) ions down the nanopipette and $Ca^{2+}$ ions from the bath towards the tip (Figure 1a, counter ion flows not shown), leading to the nucleation and growth of $CaCO_3$ at the end of the tip (*vide infra*). The growth process restricts the ion flow, which can be monitored simultaneously via the ion conductance current. After the growth period, the tip potential was switched positive (4 V) and the $CaCO_3$ dissolves (Figure 1b).

[a]     Mr. D. Perry, Mr. A.S. Parker, Mr. A. Page, Prof. Dr. P.R. Unwin
        Department of Chemistry
        University of Warwick
        Gibbet Hill Road, Coventry, CV4 7AL, United Kingdom
        E-mail: P.R.Unwin@Warwick.ac.uk
[b]     Mr. D. Perry, Mr. A. Page,
        MOAC Doctoral Training Centre
        University of Warwick
        Gibbet Hill Road, Coventry, CV4 7AL, United Kingdom
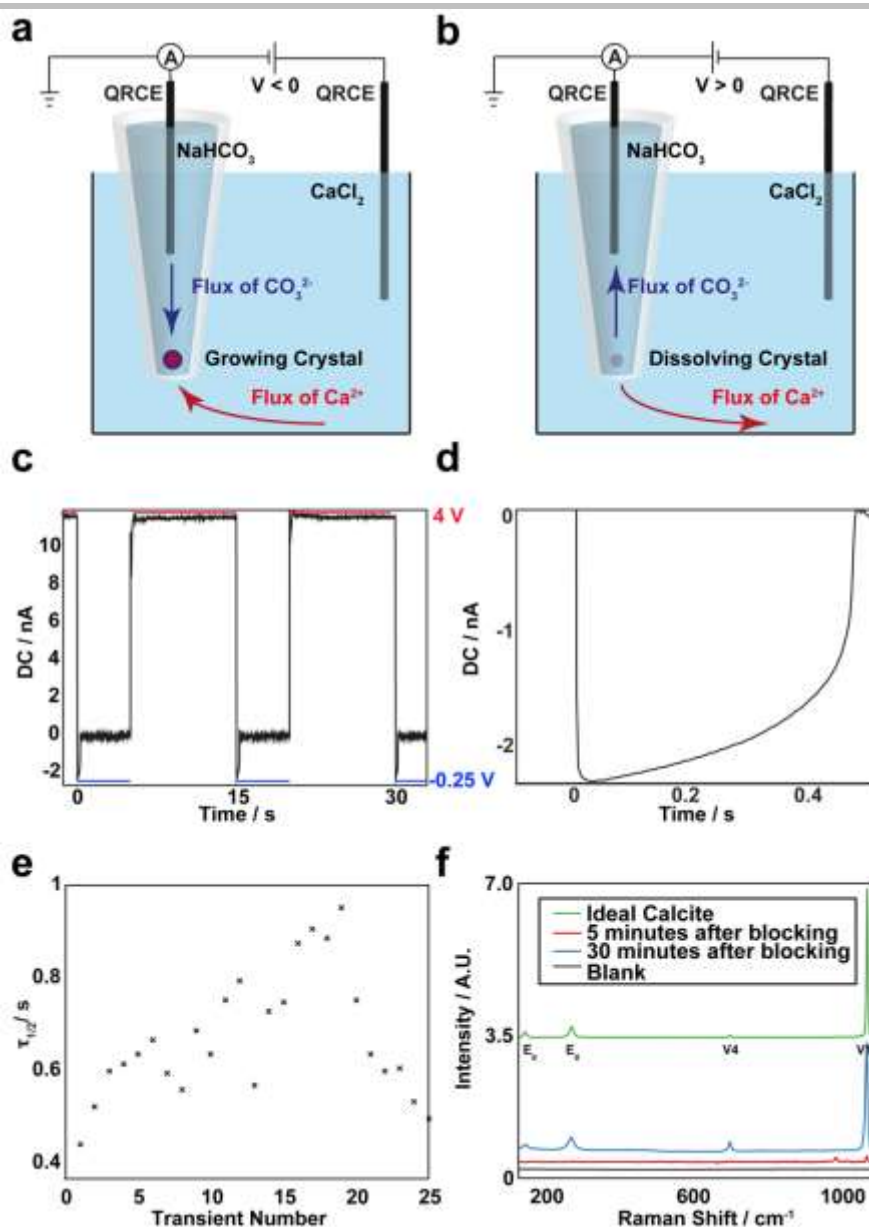        † These authors contributed equally to this work

**Figure 1.** Schematic of the principles of precipitation in a nanopipette with growth occurring with negative tip bias, **(a)**, and dissolution promoted when the polarity is reversed, **(b)**. **c)** Typical experimental blocking and unblocking events with blockages occurring with a tip bias of -0.25 V and unblocking at 4 V. **d)** Typical blocking transient with a blocking time, $\tau_{1/2}$, of about 400 ms. **e)** Variation of the blocking time, $\tau_{1/2}$, for an experimental run of 25 growth and dissolution events. **f)** Raman spectra obtained at different times during a long-time blocking measurement with the green line showing the simulated spectrum of calcite for comparison. The black line shows the spectrum of the nanopipette immersed in solution before the polarity was switched to -0.25 V and the blocking event occurred. The red spectrum was collected over a period of 5 mins (with the potential of -0.25 V still applied) after the blocking occurred and suggests at the presence of amorphous calcium carbonate. The final spectrum (blue) recorded 30 min later (-0.25 V potential still applied), shows the presence of calcite, indicating an ACC-calcite transformation.

Upon switching the bias to -0.25 V, to promote CaCO$_3$ growth, the ionic current initially has a value for an unblocked tip, but then begins to decrease, first gradually and then more rapidly with time, eventually approaching zero, corresponding to a blocked tip, as seen in Figure 1c and d. Upon switching the polarity of the bias, so that the QRCE potential in the tip was positive, the nanopipette can be seen to return to its open state, as evidenced by the large current flow in Figure 1c. It is interesting to note that the nanopipettes exhibit a rectified current-voltage response, evidenced by the open current values at 4 V and -0.25 V, respectively. This is attributed to the different solutions present in the nanopipette and bulk solution and the differing ion mobilities, although there could be an effect of the nanopipette surface charge as well. It can be also be seen that when the nanopipette

is unblocked (at 4 V applied) the current appears to be less noisy than when the nanopipette is blocked. When the nanopipette becomes blocked, ion migration would no longer drive blockage and this could lead to dissolution of the particle. Once the particle has dissolved slightly, migration would switch back on and there would be subsequent regrowth. This repeated dissolution and regrowth process could manifest as noise."

Figure 1e depicts the time taken for 50 % blockage of the ionic current from the open state, $\tau_{1/2}$, from a run of 25 crystal growth (blocking) and unblocking events with the same nanopipette. It can be seen that although there is some variation in the blocking timescale, there is no overall trend and an average blocking time of around 660 ± 250 ms is observed. The variation in timescale is most likely due to slight changes in the position

within the nanopipette where the nucleation and growth event occurs (*vide infra*), as well as the stochastic nature of nucleation. When performing these measurements, it is important to make sure that there is no trace of the grown particle for subsequent events. Consequently, unblocking times of 10 s were used for these experiments.

A significant strength of the nanopipette technique is that it is amenable to combination with additional *in situ* characterization techniques, although this was not the primary focus of this work. As an example, Raman spectroscopy was performed, focused on a 10 μm portion at the end of a nanopipette (and the surrounding solution), which confirmed that solid $CaCO_3$ was formed. Figure 1f shows typical Raman spectra obtained during and after a growth event carried out over a longer period. There were no noticeable peaks between 200 $cm^{-1}$ and 1000 $cm^{-1}$ over an acquisition time of 5 mins when the QRCE inside the nanopipette was maintained at a positive bias (4 V) with respect to the QRCE in bulk solution, so that growth would be prevented. Upon switching the bias to -0.25 V, a second Raman spectrum (5 mins acquisition time) was obtained (red line) with two peaks, one at 1085 $cm^{-1}$ and one at around 1000 $cm^{-1}$. The noticeable absence of a peak at 711 $cm^{-1}$ and the presence of that at 1085 $cm^{-1}$ suggests the formation of ACC.[12] Further, the peak at 1000 $cm^{-1}$ may be attributed to one of the metastable ACC polymorphs.[13] On, a longer timescale (after 30 mins), with the -0.25 V bias still applied, there was a phase transition to calcite evidenced by characteristic peaks[14] at 1085 $cm^{-1}$, 711 $cm^{-1}$ and the lattice peaks at 282 $cm^{-1}$ and 155 $cm^{-1}$, by comparison to the green trace of Figure 1f for calcite. These results indicate that the initial blocking of the nanopipette is likely to result from the formation of ACC, but that this eventually transforms to the more stable calcite polymorph of $CaCO_3$.[15] For the timescale of the kinetic measurements herein, which occur on a timescale of 1 s and less, the nucleation, growth and dissolution processes relate to ACC. We wish to point out that although not explored in this work. The nanopipette-based technique is well suited to ambient TEM measurements[16] and it could be worth exploring cryo-TEM in the future for further characterization of material formed.

The effect of varying the $Ca^{2+}$ concentration in the bath solution was also considered and it was found (Figure 2), that increasing the concentration of $Ca^{2+}$ initially present in solution (by adjusting the $CaCl_2$ concentration) resulted in a decrease in the

timescale of the growth process. This is attributed to the lower saturation levels that would be achieved. Although not presented, the dissolution rates were also quicker for lower $Ca^{2+}$ concentrations for the same reason. Further, in experiments where the locations of the $CO_3^{2-}$ and $Ca^{2+}$ salts were switched ($Ca^{2+}$ solution in the nanopipette, $CO_3^{2-}$ in the bath), the polarity needed to drive crystallization was reversed. Briefly, increasing the $CO_3^{2-}$ concentration resulted in shorter blocking times (data not presented).
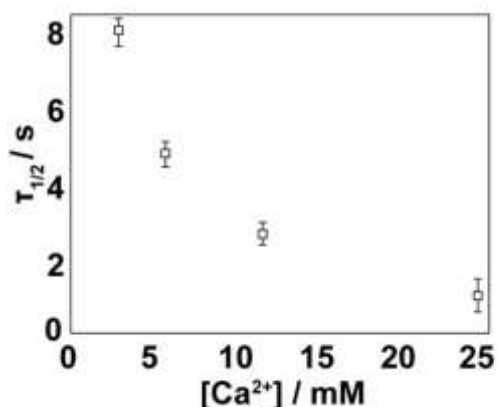


**Figure 2.** Effect of [$Ca^{2+}$] on the time required for calcium carbonate to block a nanopipette. Points are the average of 25 individual transients and the error bar is one standard deviation.

**Mixing of $Ca^{2+}$ and $CO_3^{2-}$ in a Nanopipette**

To aid understanding of the mixing and growth phenomena occurring in this system, FEM simulations of the mass transport processes due to the imposed electric field were performed with conditions similar to those that were mainly used for experiments, i.e. 125 mM $NaHCO_3$ in the nanopipette domain and 25 mM $CaCl_2$ in the bath solution (both pH 9.2, and with full speciation considered, as outlined in Table 1). The problem considered was generally similar to related nanopipette transport problems that are readily tackled with finite element method (FEM) modeling.[16-17] A schematic of the simulation domain is depicted in Figure 3a.
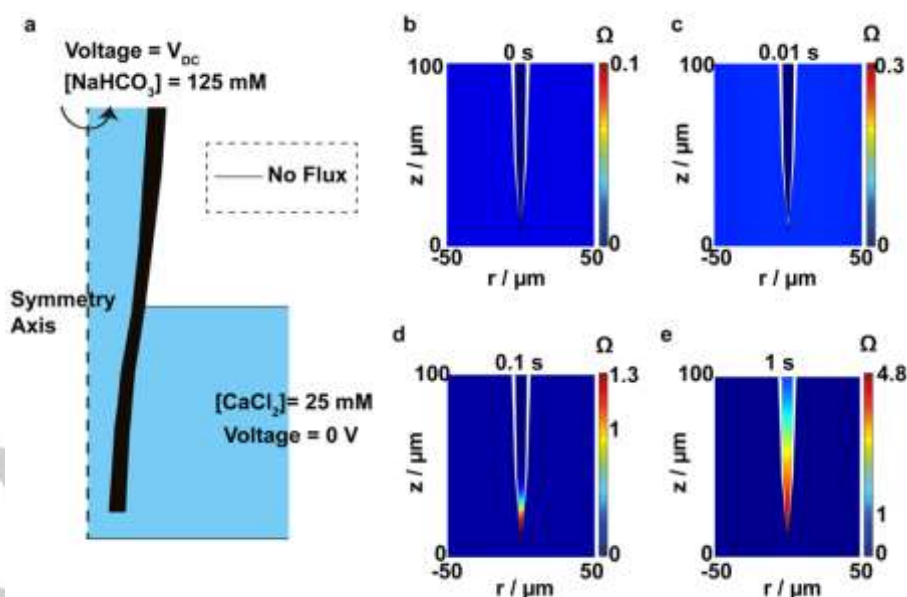


**Figure 3. a)** Schematic of FEM simulation domain used to study mixing. Simulations of the saturation level of calcium carbonate in solution, $\Omega$, at times ranging from 0 ms to 1000 ms, **(b-e)** following the application of a potential of -0.25 V to the QRCE in the nanopipette with respect to that in bulk solution.

Initially, a steady-state simulation was performed with a bias of 2 V applied to the upper boundary of the nanopipette domain. In experiments (see above), 4 V was applied in order to enhance the rate of unblocking, but it was difficult to obtain a converged solution for this condition with the computer power available. The simulation at 2 V was sufficient to illustrate the main effects with a positive QRCE potential in the tip. Using the steady-state solution for the concentration distribution with positive tip bias as the initial condition, a time-dependent simulation was then run, with the tip bias jumped to -0.25 V. Figures 3b-e depict the subsequent change in the saturation levels of CaCO$_3$ defined as:

$$\Omega = \sqrt{\frac{[Ca^{2+}] \times [CO_3^{2-}]}{K_S}} \qquad (1)$$

where [Ca$^{2+}$] and [CO$_3^{2-}$] are the concentrations of calcium and carbonate ions respectively and $K_S$ is the solubility product of calcium carbonate in water (defined in terms of concentration, rather than activity).

At the start of the simulation (before application of the driving bias), the highest value for $\Omega$ was calculated to be 0.05 and was located outside of the nanopipette. After 0.01 s with an applied bias of -0.25 V, a region at the end of the nanopipette

with a higher saturation is distinguishable, with values of up to 0.3. By 0.1 s of electric-field driven mixing, the saturation level increases above 1, i.e. the solution is supersaturated (which would promote growth). After 1 s of mixing, a supersaturation of around 5 is achieved. Figure 4a shows how the maximum

supersaturation, $\Omega_{max}$, across the simulation domain varies with time. The increase in $\Omega$ is dramatic initially, but the rate of increase gradually tails off with time. As typical blocking events lasted between 400 ms and 800 ms under these conditions, the supersaturation levels achieved were typically in the range of 3 — 5.

It is interesting to note that while the supersaturation levels change throughout the 1 s of mixing, the ionic current remains constant, after the first 0.1 ms, as shown in Figure 4b. This finding is important because it means that any change in current (experimentally) on longer timescales can be assigned to blockage of the nanopipette due to crystal growth, and the current can be used to estimate growth rates (*vide infra*).

Simulations also enabled us to elucidate the position at which growth was most likely to occur. Figure 4c shows the location of $\Omega_{max}$ within the nanopipette, measured from the nanopipette opening. When the solution was first supersaturated, time ~40 ms, this position was around 5 µm into the nanopipette, making this the most likely position for initial nucleation and growth to occur. Up to a time of about 300 ms, after applying the growth driving potential, this position increased to about 12 µm into the nanopipette, before settling at around 6 µm from the tip end at longer times.
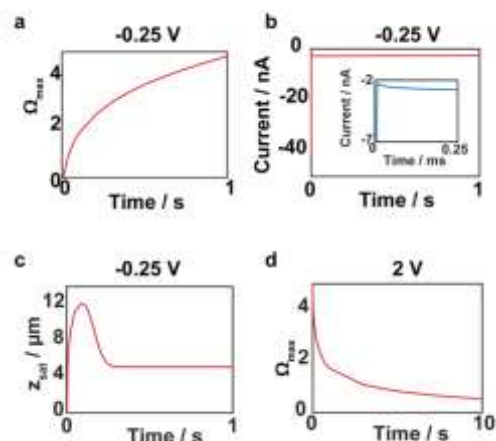


**Figure 4. a)** Maximum saturation (sampling the whole simulation domain), $\Omega_{max}$, as a function of time following the switch in the QRCE potential in the nanopipette from 2 V to -0.25 V, with respect to that in bulk solution. **b)** The simulated ionic current at a tip bias of -0.25 V can be seen to stabilize within 0.25 ms after switching the potential, inset shown with zoom to short times. **c)** Position of maximum saturation level, Z$_{sat}$, within the nanopipette (measured from the nanopipette end into the nanopipette body) as a function of time (applied potential -0.25 V). Upon switching the tip bias to be 2 V, after 600 ms of mixing at -0.25 V, the saturation can be seen to decrease rapidly with time **(d)**.

Simulations also provided justification of the time required for sufficient de-mixing of solutions, before recording the response for subsequent growth events. Figure 4d shows how the maximum value of saturation decreases when a bias of 2 V was applied after 600 ms of initial mixing. These results evidence a time of around 4 s for the saturation level to drop back below 1. This would be expected to be quicker with a higher applied bias, as used experimentally, due to the stronger electric field.[18] In the experiments, an unblocking period of 10 s was used, and the fact that there was little difference between the initial blocking transient, and those that followed (e.g. Figure 1c), is good evidence that this was sufficient time to clear the tip and reset similar starting conditions between growth events.

**Quantifying Growth Rates in a Nanopipette**

FEM simulations described above, predicted a position of around 5 µm above the nanopipette opening as the most likely location for the growth of calcium carbonate. Further FEM simulations enabled us to determine how the size of the growth product, modeled as a spherical particle, as has been observed for ACC in other work,[13] would affect the ion current. As an illustrative example, the simulation was used to analyze the experimental growth transient, presented in Figure 5a, which is representative. Simulations were performed with increasing particle size, radius, $r$ (see Experimental section) and the corresponding effect on the ionic current is observed in Figure 5b. It can be seen that the initial growth of the particle results in a small but measurable blockage of the ionic current. As the particle becomes larger, and so approaches closer to the walls of the nanopipette, the resistance increases and there is a sharp fall in the current that can pass around the growing sphere. This helps to explain the shape of the experimental transient, which typically presents a slower initial decay of the current before a sharp decrease to 0 (Figure 5a).
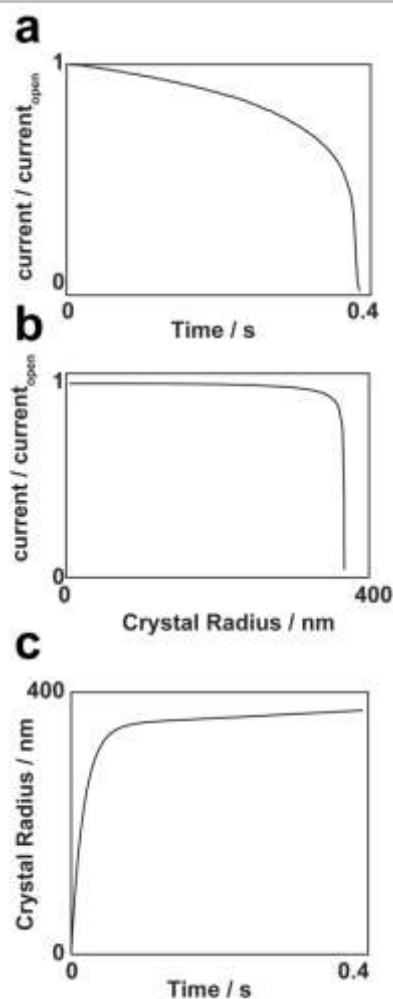
**Figure 5. (a)** Typical experimental blocking event showing how the ion conductance current (normalized by the open, maximum value) decreases with time due to blocking by CaCO₃ growth. **(b)** FEM simulation of the current-time response with a growing sphere in a nanopipette (at a height of 5 μm into the nanopipette). By combining the simulation results in **(b)** with the experimental data in **(a)**, the radius of the growing particle in a blocking event, with time can be estimated **(c)**.

By combining the data of Figure 5a and b, a plot of predicted particle radius with time can be obtained and is presented in Figure 5c. It can be seen that there is an initially high rate of linear (radial) growth, with the radius changing at a rate approaching 12 nm/ms until the particle size reaches a radius of around 300 nm and then the growth rate tails off. Note that the times presented in Figure 5 are from the point of greatest (tip open) current and do not include the initial mixing time after jumping the potential, to attain a supersaturated solution (~ 50 ms).

To determine whether the observed blocking times were reasonable, the timescale for nanopipette blocking can be compared to that expected for the flux of material to an isolated growing spherical CaCO₃ particle. For growth due to a flux, $j$, the rate of change in volume $V$, with $t$ is given by:

$$\frac{dV}{dt} = 4\pi r^2 \frac{dr}{dt} = j\frac{4\pi r^2}{\rho} \tag{2}$$

where $r$ is the radius of the particle and $\rho$ is the molar density of CaCO₃.

For a flux controlled by diffusion (maximum possible rate):

$$j = \frac{D\sqrt{K_S}(\Omega-1)}{r} \tag{3}$$

where $D$ is the diffusion coefficient of Ca²⁺ and CO₃²⁻ (assumed equal for this simple treatment). Combining equations 2 and 3 and integrating gives an expression for a growing spherical particle with time as:

$$r^2 = \frac{4D\sqrt{K_S}(\Omega-1)}{\rho}t \tag{4}$$

Using a value for $D$ of 8.5 × 10⁻⁶ cm²/s,[19] $\rho$ as 0.027 mol cm⁻³ [20] and $K_S$ as 4 × 10⁻⁷ mol cm⁻³ [21], together with $\Omega$ taken to be varying with time as per $\Omega_{max}$ from Figure 4a, this yielded an extent of growth of around 200 nm over the timescales at which blocking events were observed, a similar magnitude to the growth rates extracted from the above analysis. The transients do not strictly fit to eq. 4 because of the complex time-dependent geometry and mass-transport (diffusion and migration) to a growing nanoparticle (assumed to be spherical for simplicity) in a nanopipette, but this simple analysis highlights that the process is fast and close to mass-transport controlled.

**The Effect of Applied Bias on Blocking Rates**
The effect of changing the applied bias was briefly explored. Growth experiments were performed with varying tip bias between -1.2 V and 0 V, and $\tau_{1/2}$ values extracted (4V bias applied between each growth event, as above). It can be seen from Figure 6a that increasing negative bias from 0 V to -0.4 V, resulted in smaller values for $\tau_{1/2}$ i.e., faster CaCO₃ growth rates. However, more negative biases, beyond -0.4 V, did not result in shorter blockage times.
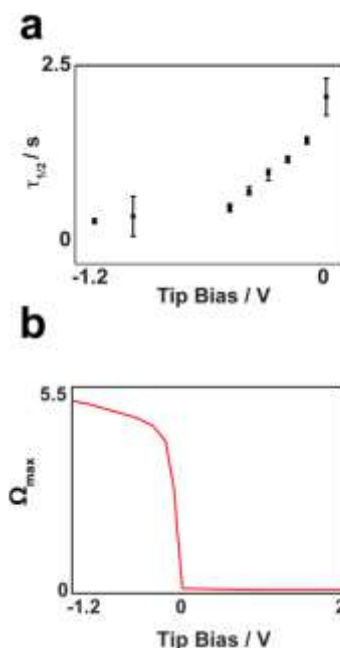


**Figure 6. a)** Experimental effect of varying the tip bias on the blocking time. As the bias is decreased below -600 mV **b)** FEM simulations reveal how the maximum saturation level, $\Omega_{max}$, varies with the tip bias. Data relate to a time of 1 s after the bias application, a similar duration to the experiments.

Simulations performed at similar tip biases revealed that the achieved saturation levels (after 1s, as illustrative) followed a similar trend to the experimental blocking times, as shown in Figure 6b. There is a relatively sharp transition (increase) in saturation level in the nanopipette tip between 0 V and -0.4 V, but

at more negative bias, the saturation level does not increase appreciably. Comparison of experiment and theory over the range of applied bias confirms that local supersaturation in the tip is the driving force for crystallization and provides insights on how the driving force may be controlled via the bias. It is however interesting to note that when there is no bias applied, the solution does eventually become locally supersaturated, because of the effects of diffusion alone and so crystal growth and blockage is possible under these conditions. This agrees with experiments performed with no net bias where the nanopipettes were observed to block.

**Effect of Additives**

There is great interest in assessing the impact of additives on CaCO$_3$ formation, particularly in relation to scaling,[12, 22] and, as such, novel methods of assessing and being able to compare the effects of additive are very valuable. The nanopipette method offers a robust platform to quickly assess and rank such growth inhibitors. Maleic acid (MA), which exists as the dianion under typical CaCO$_3$ growth conditions (herein at pH 9.2), is one such growth inhibitor that has been studied and shown to be effective for both dissolution and growth inhibition of calcite.[23] The mechanism of the inhibitory action of MA has been debated, with one hypothesis being that it acts as a chelating agent, binding to Ca$^{2+}$ ions to desupersaturate solutions.[24] The alternative mode of action is that MA acts on the calcite surface.[23b] Experimental runs of 25 growth (and unblocking) events, were performed as outlined above at each of a series of MA concentrations present in the bath solution. The same nanopipette was used and the bath simply changed. This eliminates error from small changes in the nanopipette geometry and highlights how hundreds of quantitative growth measurements can be made quickly, making this a powerful screening methodology.

Figure 7a shows typical ion conductance current-time transients for different concentrations of MA (up to 8 mM) in the bath solution. It can be seen that increasing the concentration of MA in solution results in significantly longer times required for full blocking of the nanopipette, with the blocking time (CaCO$_3$ growth rate) being one to two orders of magnitude longer in the presence of 8 mM MA than without. Figure 7b suggests a strong effect of MA concentration on the mean value of $\tau_{1/2}$. Furthermore, through careful design of the initial experimental concentrations, it is possible to obtain some mechanistic information about the MA mode of action. Specifically, were MA solely acting as a chelating agent, 8 mM MA would (at most) desupersaturate the bath solution by 8 mM of Ca$^{2+}$ ions. An experimental run was thus performed with 17 mM CaCl$_2$ present in the bath solution. This experiment yielded a value for $\tau_{1/2}$ of 2.1 ± 0.1 as compared to the value of $\tau_{1/2}$ with 8 mM MA of around 16 s. Thus, MA does not act solely as a Ca$^{2+}$ chelation agent, but has significant surface effects, consistent with AFM measurements of calcite growth in the presence of MA.[23b]

To highlight the application of this technique for fast additive screening, several different known growth inhibitors were incorporated into the nanopipette bath solution to observe the subsequent effect on crystallization times. These were citrate, aspartic acid (Asp), polyaspartic acid (PAsp), polystyrene sulfonate (PSS), bis(2-ethylhexyl)sulfosuccinate (AOT), sulfate and magnesium all of which are known to have some effect on CaCO$_3$ crystallization and whose structures are presented in Figure 7d .[12] The addition of 8 mM each of these different additives to a set of baths allowed their efficacy for crystal growth inhibition to be rapidly screened. The resulting average blockings time are summarized in Figure 7c and the trend – for the same additives - is consistent with bulk studies,[12] although the nanopipette method reveals the additive effect much more quickly. This methodology paves the way for the rapid screening of crystal growth and dissolution additives.
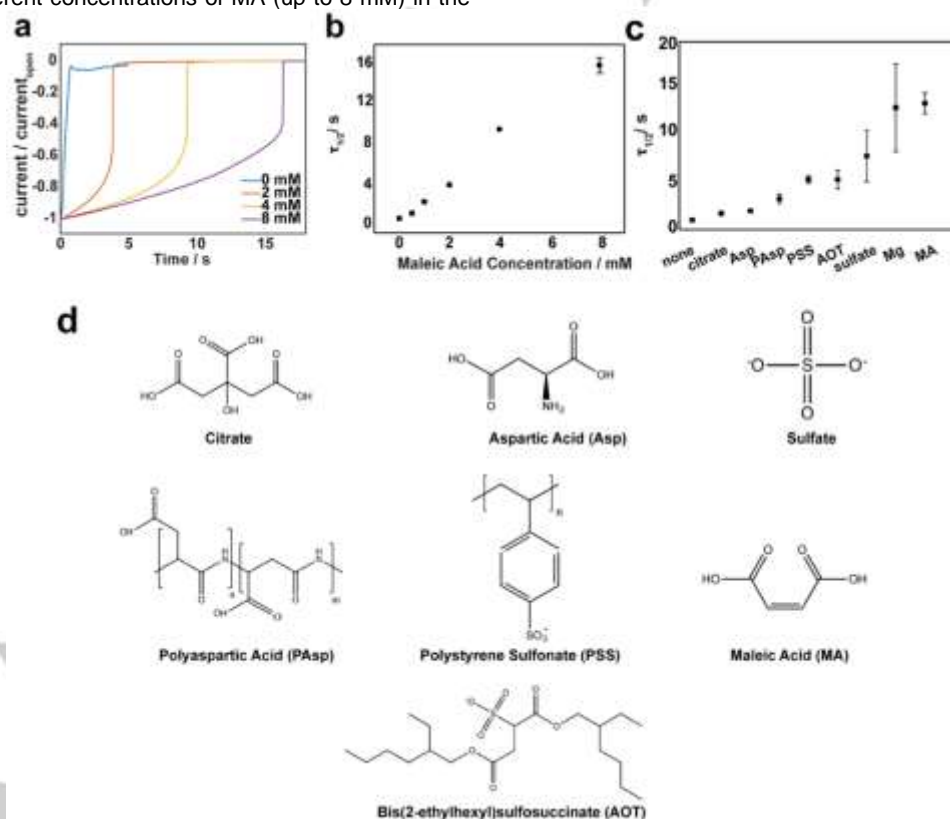


**Figure 7. a)** Example current-time transients with different concentrations of the additive, MA as indicated. **b)** Summary plot of mean values of $\tau_{1/2}$ for 25 runs in each case, with the error bars representing the standard error of the mean. **c)** Mean blockage time over a run of 25 growth events for each of the different additives. **d)** Structures of tested additives.

## Conclusions

Nanopipettes, under bias control, provide a powerful and robust and quantitative platform for the electrochemical (conductimetric) monitoring of crystal growth events on the nanoscale. By tuning the bias applied between a QRCE in a nanopipette and one positioned outside in a bath solution, crystal formation can be driven at the end of a nanopipette, and the corresponding current-time response can be used to extract growth kinetics. The deposit can be removed subsequently by reversing the polarity of the applied bias and the system is reset to perform the next growth experiment. The power of this technique is increased further through combination with other methods, most notably Raman spectroscopy, which can provide diagnostic information about the product formed in-situ. We further anticipate that other complementary techniques such as cryo-TEM could also be incorporated in future work. The studies herein relate to the nucleation and growth of amorphous calcium carbonate, which is an important precursor involved in the formation of other $CaCO_3$ polymorphs.

The approach described has been supported by a detailed FEM model, which provides key information about the mixing times needed for product formation as well as the supersaturation levels achievable. Furthermore, the effects of applied bias have been explored by combining experimental and simulation results, to reveal how the technique can be used optimally to drive and control crystallization events.

Finally, the power of this technique in the study of additives has been highlighted. Maleic acid has been revealed as a potent inhibitor of $CaCO_3$ growth, which has a strong concentration-dose response, and the method has been employed to produce a rank order of additive efficacy. As the search for effective crystal growth additives is challenging and somewhat time consuming with conventional batch methods, the nanopipette format is particularly attractive and opens up important new possibilities for rapid screening.

## Experimental Section

**Solutions.** All solutions were made up using 18.2 MΩ cm water (Millipore Inc.) and chemicals used were purchased from Sigma Aldrich. The nanopipette contained 125 mM $NaHCO_3$ electrolyte solution for experiments and the bath contained 25 mM $CaCl_2$, unless stated otherwise. For inhibitor studies, maleic acid (MA) was added to the bath solution at concentrations ranging from 0.5 mM to 8 mM. Studies with other inhibitors were performed with concentrations of 8 mM added to a series of bath solutions. For all experiments, solutions were adjusted to pH 9.2.

**Nanopipettes.** Nanopipettes were fabricated using quartz glass capillaries with filaments (outer diameter 1.0 mm, inner diameter 0.5 mm, custom manufactured, Friedrich and Dimmock) using a laser puller (P-2000, Sutter Instruments; parameters of: Line 1: Heat 750, Fill 4, Vel 30, Del 150, Pull 80; Line 2: Heat 650, Fil 3, Vel 40, Del 135, Pull 150) to give a tip opening diameter of approximately 40-60 nm (determined accurately).[16]

**Instrumentation.** The electrometer and current-voltage converter used were home built, while the user control of voltage output and data collection was via custom made programs in LabVIEW (2013, National Instruments) through an FPGA card (7852R, National Instruments).

**Bias Driven Crystallization Experiments.** Typical crystallization experiments involved filling the nanopipette with $NaHCO_3$ solution, to serve as both supporting electrolyte and a source of $CO_3^{2-}$ ions (adjusted to pH 9.2 by addition of NaOH), along with a chloridized silver wire, which served as a QRCE. The nanopipette was immersed in a solution of $CaCl_2$ containing a second Ag/AgCl QRCE. To drive crystallization, a negative bias was applied to the nanopipette QRCE relative to the bulk electrode. To unblock the nanopipette for subsequent experiments a positive bias (4 V) was applied. Lower magnitude unblocking potentials were tested (results not presented herein) and resulted in unblocking over a longer timescale. The open circuit potential was measured using a custom built high impedance voltage follower and was found to be -40 mV at the nanopipette QRCE with respect to the bulk QRCE. As this was considerably smaller than the blocking and unblocking biases applied in experiments and simulations (*vide infra*), all values for potential stated are uncorrected but this could be easily accounted for.

Each experimental run consisted of 25 blocking and unblocking events and all quoted blocking times, $\tau_{1/2}$, referred to herein, are measured from the time of the voltage switch to the time the current dropped to half its maximum value (open tip current at the same potential). All experiments were performed at room temperature, measured to be 25 °C.

**FEM Simulations.** A 2D axisymmetric model of the nanopipette in bulk solution was constructed in Comsol Multiphysics (v. 5.2) with the Transport of Diluted Species and Electrostatics modules. A schematic of the simulation domain and the equations solved is presented in Figure 3a. The dimensions of the nanopipette were extracted from TEM images of nanopipettes and these were faithfully reproduced in the model so that the experimental geometry was mimicked precisely.[16] The equations and boundary conditions solved in the FEM simulations were as in previous work,[3c, 16] and outlined in the manuscript but additionally with calcium carbonate speciation incorporated with parameters shown in Table 1.[25] Ionic transport is assumed to follow the classical Nernst-Planck relationship, where the flux $J_i$ of species, $i$, is given as:

$$J_i = -D_i \nabla c_i - z_i \frac{F}{RT} D_i c_i \nabla f \qquad (5)$$

and the Poisson equation describes the electrical potential $\phi$:

$$\nabla^2 f = -\frac{F}{\varepsilon \varepsilon_0} \sum_i z_i c_i \qquad (6)$$

where $c_i$ denotes the species concentration, while $D_i$, $z_i$, $F$, $R$, $T$, $\varepsilon$ and $\varepsilon_0$ specify constants: system diffusion coefficient of $i$, its charge number, the Faraday constant, gas constant, temperature, relative permittivity and vacuum permittivity, respectively.

The $CaCl_2$ concentration was set as 25 mM to the rightmost boundary of the bulk domain with the top of the nanopipette domain held at 125 mM $NaHCO_3$. The bias, $V_{DC}$, was applied to the bulk nanopipette domain and was usually -0.25 V for the study of crystal growth or 2 V for the study of subsequent unmixing. There was a no flux condition at the walls of the nanopipette and bulk domain boundary.

To extract growth rates, a FEM simulation was run with spherical particles of different radius in the nanopipette, positioned 5 μm from the nanopipette opening into the nanopipette. The percentage block off of current was compared to experimental transients to extract an estimated size for the crystal varying with time.

**Table 1** Calcium carbonate speciation parameters[25]

| Eq | Reaction | pK |
|---|---|---|
| 7 | $CO_2 + H_2O \rightleftharpoons H_2CO_3$ | 1.466 |
| 8 | $H_2CO_3 \rightleftharpoons H^+ + HCO_3^-$ | 6.351 |
| 9 | $HCO_3^- \rightleftharpoons H^+ + CO_3^{2-}$ | 10.33 |
| 10 | $CaHCO_3^+ \rightleftharpoons Ca^{2+} + HCO_3^-$ | 1.015 |
| 11 | $CaCO_{3(aq)} \rightleftharpoons Ca^{2+} + CO_3^{2-}$ | 3.2 |
| 12 | $H_2O \rightleftharpoons OH^- + H^+$ | 13.997 |

**Raman Spectroscopy.** *In-situ* micro-Raman spectra were collected from a 10 μm long region at the end of a nanopipette that had undergone a blocking event, using a Raman microscope (Renishaw, UK) fitted with a Charge Coupled Device (CCD) detector and a 514.5 nm Ar+ laser. A 20X lens was employed.

## Acknowledgements

[1]     a) Y. Fu, H. Tokuhisa, L. A. Baker, *Chem. Commun.* **2009**, 4877-4879; b) P. Actis, A. C. Mak, N. Pourmand, *Bioanal. Rev.* **2010**, *1*, 177-185; c) J. C. Byers, B. Paulose Nadappuram, D. Perry, K. McKelvey, A. W. Colburn, P. R. Unwin, *Anal. Chem.* **2015**, *87*, 10450-10456; d) M. A. Edwards, S. R. German, J. E. Dick, A. J. Bard, H. S. White, *ACS Nano* **2015**, *9*, 12274-12282; e) D. A. Holden, J. J. Watkins, H. S. White, *Langmuir* **2012**, *28*, 7572-7577.

[2]     a) A. Bruckbauer, P. James, D. Zhou, J. W. Yoon, D. Excell, Y. Korchev, R. Jones, D. Klenerman, *Biophys. J.* **2007**, *93*, 3120-3131; b) A. Bruckbauer, L. Ying, A. M. Rothery, D. Zhou, A. I. Shevchuk, C. Abell, Y. E. Korchev, D. Klenerman, *J. Am. Chem. Soc.* **2002**, *124*, 8810-8811; c) A. P. Ivanov, P. Actis, P. Jönsson, D. Klenerman, Y. Korchev, J. B. Edel, *ACS Nano* **2015**, *9*, 3587-3595.

[3]     a) N. Ebejer, A. G. Güell, S. C. Lai, K. McKelvey, M. E. Snowden, P. R. Unwin, *Annu. Rev. Anal. Chem.* **2013**, *6*, 329-351; b) D. Perry, R. Al Botros, D. Momotenko, S. L. Kinnear, P. R. Unwin, *ACS Nano* **2015**, *9*, 7266-7276; c) D. Perry, B. Paulose Nadappuram, D. Momotenko, P. D. Voyias, A. Page, G. Tripathi, B. G. Frenguelli, P. R. Unwin, *J. Am. Chem. Soc.* **2016**, *138*, 3152-3160; d) Q. Li, S. Xie, Z. Liang, X. Meng, S. Liu, H. H. Girault, Y. Shao, *Angew. Chem. Int. Ed.* **2009**, *48*, 8010-8013; e) C. Kranz, *Analyst* **2014**, *139*, 336-352.

[4]     P. Actis, M. M. Maalouf, H. J. Kim, A. Lohith, B. Vilozny, R. A. Seger, N. Pourmand, *ACS Nano* **2013**, *8*, 546-553.

[5]     E. M. Yuill, W. Shi, J. Poehlman, L. A. Baker, *Anal. Chem.* **2015**, *87*, 11182-11186.

[6]     C. R. Heath, B. C. S. Leadbeater, M. E. Callow, *J. Appl. Phycol.*, *7*, 367-380.

[7]     a) S.-S. Wang, A.-W. Xu, *Cryst. Growth Des.* **2013**, *13*, 1937-1942; b) A. B. Rodríguez-Navarro, P. Marie, Y. Nys, M. T. Hincke, J. Gautron, *J. Struct. Biol.* **2015**, *190*, 291-303.

[8]     Y. Miyazaki, J. D. Reimer, *ZooKeys* **2015**, 1.

[9]     K. S. Lackner, *Science* **2003**, *300*, 1677-1678.

[10]    a) B. R. Soktoev, L. P. Rikhvanov, I. A. Matveenko, *IOP Conference Series: Earth and Environmental Science* **2015**, *27*, 012042; b) M. F. Butler, N. Glaser, A. C. Weaver, M. Kirkland, M. Heppenstall-Butler, *Cryst. Growth Des.* **2006**, *6*, 781-794; c) G. A. Tribello, C. Liew, M. Parrinello, *J. Phys. Chem. B* **2009**, *113*, 7081-7085.

[11]    B. Vilozny, P. Actis, R. A. Seger, N. Pourmand, *ACS Nano* **2011**, *5*, 3191-3197.

[12]    J. Ihli, Y.-Y. Kim, E. H. Noel, F. C. Meldrum, *Adv. Funct. Mater.* **2013**, *23*, 1575-1585.

[13]    M. M. Tlili, M. B. Amor, C. Gabrielli, S. Joiret, G. Maurin, P. Rousseau, *J. Raman Spectrosc.* **2002**, *33*, 10-16.

[14]    G. Behrens, L. T. Kuhn, R. Ubic, A. H. Heuer, *Spectrosc. Lett.* **1995**, *28*, 983-995.

[15]    a) M. H. Nielsen, S. Aloni, J. J. De Yoreo, *Science* **2014**, *345*, 1158-1162; b) P. Bots, L. G. Benning, J.-D. Rodriguez-Blanco, T. Roncal-Herrero, S. Shaw, *Cryst. Growth Des.* **2012**, *12*, 3806-3814.

[16]    D. Perry, D. Momotenko, R. A. Lazenby, M. Kang, P. R. Unwin, *Anal. Chem.* **2016**, *88*, 5523–5530.

[17]    L. Ying, S. S. White, A. Bruckbauer, L. Meadows, Y. E. Korchev, D. Klenerman, *Biophys. J.* **2004**, *86*, 1018-1027.

[18]    a) C. A. Morris, A. K. Friedman, L. A. Baker, *Analyst* **2010**, *135*, 2190-2202; b) R. W. Clarke, S. S. White, D. Zhou, L. Ying, D. Klenerman, *Angew. Chem. Int. Ed.* **2005**, *44*, 3747-3750.

[19]    W. M. Haynes, *CRC handbook of chemistry and physics*, CRC press, **2014**.

[20]    J. Ihli, W. C. Wong, E. H. Noel, Y.-Y. Kim, A. N. Kulak, H. K. Christenson, M. J. Duer, F. C. Meldrum, *Nature communications* **2014**, *5*.

[21]    L. Brečević, A. E. Nielsen, *J. Crys. Growth* **1989**, *98*, 504-510.

[22]    a) S. M. Hamza, S. K. Hamdona, *J. Chem. Soc. Faradat T.* **1992**, *88*, 2713-2716; b) Z. Amjad, *Mineral scale formation and inhibition*, Springer Science & Business Media, **2013**; c) M. Sancho-Tomás, S. Fermani, M. A. Durán-Olivencia, F. Otálora, J. Gómez-Morales, G. Falini, J. García-Ruiz, *Cryst. Growth Des.* **2013**, *13*, 3884-3891; d) J. N. Bracco, M. C. Grantham, A. G. Stack, *Cryst. Growth Des.* **2012**, *12*, 3540-3548.

[23]    a) Z. Amjad, P. G. Koutsoukos, *Desalination* **2014**, *335*, 55-63; b) P. S. Dobson, L. A. Bindley, J. V. Macpherson, P. R. Unwin, *ChemPhysChem* **2006**, *7*, 1019-1021.

[24]    a) D. Changa, *J. Am. Oil Chem. Soc.* **1983**, *60*, 618-622; b) T. Kumar, S. Vishwanatham, S. Kundu, *J. Petrol. Sci. Eng.* **2010**, *71*, 1-7.

[25]    B. P. Nadappuram, K. McKelvey, R. Al Botros, A. W. Colburn, P. R. Unwin, *Anal. Chem.* **2013**, *85*, 8070-8074.

**Entry for the Table of Contents** (Please choose one layout)

Layout 2:

## ARTICLE
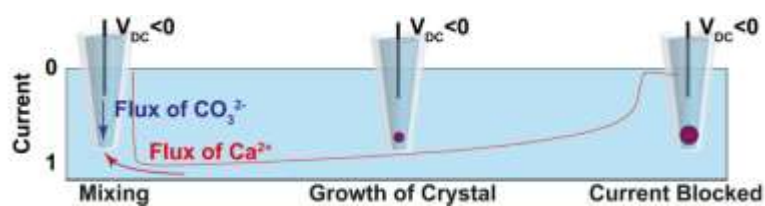


*D. Perry, A.S. Parker, A. Page, P.R. Unwin\**

Title: Electrochemical Control of Calcium Carbonate Crystallization and Dissolution in Nanopipettes

**Mix it up and Start Again**: A novel electrochemical method to study growth and dissolution kinetics at the nanoscale, as well as to quickly screen additives.